THE JOURNAL OF BIOLOGICAL CHEMISTRY VOL. 285, NO. 8, pp. 5792–5801, February 19, 2010

Post-translational Modification of Ribosomal Proteins

STRUCTURAL AND FUNCTIONAL CHARACTERIZATION OF RimO FROM THERMOTOGA MARITIMA, A RADICAL S-ADENOSYLMETHIONINE METHYLTHIOTRANSFERASE[S]

Received for publication, September 14, 2009, and in revised form, December 7, 2009 Published, JBC Papers in Press, December 9, 2009, DOI 10.1074/jbc.M109.065516

Simon Arragain[‡], Ricardo Garcia-Serres[‡], Geneviève Blondin[‡], Thierry Douki[§], Martin Clemancey[‡], Jean-Marc Latour[‡], Farhad Forouhar[¶‖], Helen Neely[¶‖], Gaetano T. Montelione[¶‡‡], John F. Hunt[¶‖1], Etienne Mulliez[‡], Marc Fontecave[‡§§], and Mohamed Atta[‡2]**

*From the [‡]Institut de Recherches en Technologie et Sciences pour le Vivant-Laboratoire de Chimie et Biologie des Métaux (iRTSV-LCBM), UMR 5249, CEA-CNRS-UJF, Commissariat à l'Energie Atomique Grenoble, 17 Avenue des Martyrs, 38054 Grenoble Cedex 09, France, [§]DSM/INaC/SCIB, UMR E3, CEA-UJF, Laboratoire Lésions des Acides Nucléiques, Commissariat à l'Energie Atomique Grenoble, 38054 Grenoble Cedex 09, France, the [¶]Northeast Structural Genomics Consortium, Columbia University, New York, New York 10027, the [‖]Department of Biological Sciences, Columbia University, New York, New York 10027, the **Center for Advanced Biotechnology and Medicine and Department of Molecular Biology and Biochemistry, Rutgers University, Piscataway, New Jersey 08854, the [‡‡]Department of Biochemistry, Robert Wood Johnson Medical School, University of Medicine and Dentistry of New Jersey, Piscataway, New Jersey 08854, and the [§§]Collège de France, 11 place Marcellin-Berthelot, 75005 Paris, France*

Post-translational modifications of ribosomal proteins are important for the accuracy of the decoding machinery. A recent *in vivo* study has shown that the *rimO* gene is involved in generation of the 3-methylthio derivative of residue Asp-89 in ribosomal protein S12 (Anton, B. P., Saleh, L., Benner, J. S., Raleigh, E. A., Kasif, S., and Roberts, R. J. (2008) *Proc. Natl. Acad. Sci. U. S. A.* 105, 1826–1831). This reaction is formally identical to that catalyzed by MiaB on the C2 of adenosine 37 near the anticodon of several tRNAs. We present spectroscopic evidence that *Thermotoga maritima* RimO, like MiaB, contains two [4Fe-4S] centers, one presumably bound to three invariant cysteines in the central radical *S*-adenosylmethionine (AdoMet) domain and the other to three invariant cysteines in the N-terminal UPF0004 domain. We demonstrate that holo-RimO can specifically methylthiolate the aspartate residue of a 20-mer peptide derived from S12, yielding a mixture of mono- and bismethylthio derivatives. Finally, we present the 2.0 Å crystal structure of the central radical AdoMet and the C-terminal TRAM (tRNA methyltransferase 2 and MiaB) domains in apo-RimO. Although the core of the open triose-phosphate isomerase (TIM) barrel of the radical AdoMet domain was conserved, RimO showed differences in domain organization compared with other radical AdoMet enzymes. The unusually acidic TRAM domain, likely to bind the basic S12 protein, is located at the distal edge of the radical AdoMet domain. The basic S12 protein substrate is likely to bind RimO through interactions with both the TRAM domain and the concave surface of the incomplete TIM barrel. These biophysical results provide a foundation for understanding the mechanism of methylthioation by radical AdoMet enzymes in the MiaB/RimO family.

Ribosomes are large ribonucleoprotein complexes that catalyze the peptidyltransferase reaction in protein synthesis and are thus responsible for the translation of transcripts encoded in the cellular genome. Detailed analyses of eukaryote and prokaryote ribosomes by peptide mass spectrometry provide insights into the composition of ribosomal proteins and show a high degree of post-translational modifications (1). These modifications are believed to extend molecular structures beyond the limits imposed by the 20 genetically encoded amino acids (2). For example, the *Escherichia coli* ribosomal protein S12 is shown to be post-translationally modified through 3-methylthiolation of the Asp-89[3] residue (Scheme 1*A*), a modification believed to improve translational accuracy (3, 4). Recently, the *yliG* gene (later named *rimO* for ribosomal modification O) has been shown to be responsible for this reaction *in vivo* (5). The protein encoded by this gene, RimO, contains in its central part the highly conserved cysteine triad Cys-*XXX*-Cys-*XX*-Cys, which is the hallmark of the radical AdoMet[4] superfamily (Scheme 1*B*) (6).

Radical AdoMet enzymes share a common mechanism that utilizes a $[4Fe\text{-}4S]^{2+/1+}$ cluster chelated by the three cysteines of the triad and by AdoMet to initiate, under reducing conditions, a radical reaction mediated by a 5′-deoxyadenosyl radical arising from the reductive cleavage of the bound AdoMet (7, 8). This radical abstracts a hydrogen atom from a properly positioned substrate creating a substrate-based carbon radical. In the formation of 3-methylthioaspartate at Asp-89 of the S12 protein (ms-D89-S12), this radical is supposed to be located on the C3 of Asp-89, and then the site becomes successively thiolated and methylated (9).

Several other radical AdoMet enzymes besides RimO catalyze the thiolation of substrates, including a tRNA-methylthio-

[S] The on-line version of this article (available at http://www.jbc.org) contains supplemental Figs. 4–10.

The atomic coordinates and structure factors (code 2QGQ) have been deposited in the Protein Data Bank, Research Collaboratory for Structural Bioinformatics, Rutgers University, New Brunswick, NJ (http://www.rcsb.org/).

[1] To whom correspondence may be addressed. E-mail: jfhunt@biology.columbia.edu.

[2] To whom correspondence may be addressed. Tel.: 33-438789115; Fax: 33-438789124; E-mail: mohamed.atta@cea.fr.

[3] According to the UniProt data bank (P0A7S3), the modified Asp residue of protein S12 is located on Asp-89 and not on Asp-88 as erroneously specified in Kowalak *et al.* (4) and Anton *et al.* (5).

[4] The abbreviations used are: AdoMet, *S*-adenosylmethionine; msD89-S12, 3-methylthioaspartate at Asp-89 of S12 protein; AdoH, 5′-deoxyadenosine; TRAM, tRNA methyltransferase 2 and MiaB; HPLC, high pressure liquid chromatography; CAPS, 3-(cyclohexylamino)propanesulfonic acid; mT, millitesla; PDB, Protein Data Bank; r.m.s.d., root mean square deviation; T, tesla.

transferase enzyme (MiaB), biotin synthase (BioB), and lipoic acid synthase (LipA) (10, 11). RimO and MiaB share a common domain organization consisting of an N-terminal UPF0004 domain that is ~135 residues in length, a central radical AdoMet domain of ~235 residues in length containing the radical AdoMet cysteine triad, and a C-terminal TRAM domain of ~60 residues in length (Scheme 1*B*) (12). The domain organization of BioB and LipA differs. A comprehensive analysis of 475 different microbial genomes suggests that RimO and MiaB belong to an enzyme family with conserved domain architecture that includes 16 distinct groups in eubacteria alone.[5] As many as three different paralogs in the RimO/MiaB family are encoded in some single genomes in this data set.

The UPF0004 domain has not been characterized structurally, but it also contains three highly conserved cysteine residues. The very high sequence homology in the UPF0004 domain of MiaB and RimO strongly suggests that RimO binds two [4Fe-4S] clusters as is the case for MiaB (Scheme 1*B*) (13). BioB and LipA, the two other radical AdoMet thiolating enzymes, also contain three conserved cysteines, but both their spacing and location in the sequence differ from those of MiaB and RimO. It is generally considered that in these systems (MiaB, LipA, and BioB) the second cluster serves as a source of sulfur atoms for substrate thiolation (11). However, more experimental data are needed to support this hypothesis, as these systems are not catalytic *in vitro* even in the presence of the iron-sulfur cluster assembly machineries.

The sequence similarity between MiaB and RimO is also apparent in the C-terminal TRAM domain. In MiaB the latter is proposed to be involved in RNA binding as it has been shown for diverse enzymes (12, 14). The hypothesis that RimO methylthiolates a protein rather than an RNA substrate suggests that the binding specificity of the TRAM domain could be substantially altered in RimO compared with MiaB and the other RNA-modifying enzymes containing this domain.

In this work, we show that RimO from *Thermotoga maritima* indeed contains, in addition to the radical AdoMet [4Fe-4S]$^{2+/1+}$, a second, N-terminal [4Fe-4S]$^{2+/1+}$ cluster. The spectroscopic and redox properties of each [4Fe-4S] cluster have been investigated and shown to display distinctive signatures. In addition we set up the first *in vitro* assay for the RimO-dependent introduction of a methylthio group at the C3 aspartate residue of a 20-amino acid peptide mimicking the active site of the S12 physiological substrate, strongly supporting the hypothesis that this segment of S12 is a physiological substrate for methylthiolation by RimO. Finally, we have presented the crystal structure of the central radical AdoMet and C-terminal TRAM domains from the apo-form of *T. maritima* RimO, which provides important hints as to how the enzyme recognizes its protein substrate and mediates the methylthiolation reaction.

MATERIALS AND METHODS

Strains—E. coli DH5α was used for routine DNA manipulations. *E. coli* BL21 CodonPlus(DE3)-RIL^{TM} (Stratagene) was used to produce the recombinant protein RimO.

Expression and Purification of T. maritima RimO—Protein expression was conducted in LB medium at 37 °C using the *E. coli* BL21 CodonPlus(DE3)-RIL^{TM} as described previously (15). RimO protein was purified under aerobic conditions and contained low amounts of Fe-S clusters. The apo-form was obtained by exposure to EDTA (10 mM) under reducing conditions (5 mM sodium dithionite) as described previously (15).

Reconstitution of the Apo-form of T. maritima RimO—Fe-S cluster reconstitution into *T. maritima* RimO was carried out under strictly anaerobic conditions in a Jacomex NT glove box containing less than 2 ppm O_2. Following incubation of the apo-protein with 5 mM dithiothreitol for 10 min, a 10-fold molar excess of ferrous ammonium sulfate ($Fe(NH_4)_2(SO_4)_2$) was added followed by the addition of a 12-fold molar excess of L-cysteine and a catalytic amount of the *E. coli* cysteine desulfurase CsdA. Holo-RimO was purified using a published procedure (13). A slightly modified protocol was used to prepare Mössbauer samples starting with ^{57}Fe-enriched $FeCl_3$ reduced *in situ* with 4 mM dithiothreitol.

Peptide Synthesis—The 20-mer peptide LVRGGRVK-**D**LPGVRYKIIRG, which contains the sequence surrounding Asp-89 of the S12 protein physiological substrate, was synthesized by ProteoGenix (Strasbourg, France). Analytical HPLC, performed on a 0.46 × 25-cm Zorbax C4 column (Agilent), showed that the purity of the peptide was >95%.

In Vitro Enzyme Assay—The assay mixture (50 μl) contained a 30 μM 20-mer peptide substrate and a 6 μM reconstituted RimO protein in 0.2 mM AdoMet, 2 mM dithionite, and 100 mM Tris-Cl, pH 7.5. The reaction was carried out at 50 °C under anaerobic conditions. After a 60-min reaction time, two aliquots (30 and 15 μl) of the solution were transferred into Eppendorf tubes, and the reaction was stopped by exposure to air followed by flash-freezing in liquid nitrogen. With the first aliquot (30 μl), conversion of the peptide substrate into the thiomethylated product was quantified by HPLC coupled to tandem mass spectrometry (HPLC-MS/MS) (see below). For the second aliquot (15 μl), the volume was then adjusted to 100 μl with water, and the solution was centrifuged at room temperature for 10 min at 14,000 rpm. The supernatant was injected onto an HPLC Zorbax SB-C18 column equilibrated with 0.1% trifluoroacetic acid. A linear gradient from 0 to 28% acetonitrile in 0.1% trifluoroacetic acid was run at 1 ml/min for 15 min. *S*-Adenosylhomocysteine and 5′-deoxyadenosine (AdoH) were detected at 260 nm and identified by comparing their elution times (12 and 14 min, respectively) with that of commercial samples.

Protein, Iron, Labile Sulfide, and Activity Assays—Holo-RimO protein concentration was determined by quantitative amino acid analysis giving an extinction coefficient at 280 nm of 100 mM^{-1} cm^{-1} translating into a 2.3–2.4 overestimation factor when using the standard Bradford assay calibrated with bovine serum albumin. Protein-bound iron was determined by a modified W. W. Fish procedure (16). Labile sulfide was determined according to the standard procedure (17).

Mass Spectrometry Analysis—HPLC-tandem mass spectrometry analyses were performed with a 1100 Agilent chromatographic system coupled with an API 3000 triple quadrupolar apparatus (PerkinElmer Life Sciences) equipped with a

[5] S. Handelman and J. F. Hunt, manuscript in preparation.

turbo ionspray electrospray source used in the positive mode. HPLC separation was carried out with a 2.1Í150-mm C4 silica gel (5-mm particle size) column (Grace Davison Discovery Sciences, Deerfield, IL) and a gradient of acetonitrile containing 0.1% formic acid in a 0.1% formic acid solution as the mobile phase. The proportion of acetonitrile rose from 0 to 30% over the first 30 min and further increased to 60% in 5 min. Mass spectra were recorded between $m/z = 380$ and 1130. For quantitative analyses, chromatograms corresponding to the mass of the +5, +4, and +3 charge states of the peptide and its monomethylthio and bismethylthio derivatives were extracted. The area of the peaks were determined and summed for a same compound. A comparison of the values obtained for each analyte reflected the concentration of each in the reaction mixture.

Spectroscopic Characterization of Fe-S Centers—UV-visible absorption spectra were recorded in quartz cuvettes (optic path 1 cm) under anaerobic conditions in a glove box on a XL-100 Uvikon spectrophotometer equipped with optical fibers. Mössbauer spectra were recorded at 4.2 K, either on a low field Mössbauer spectrometer equipped with a Janis SVT-400 cryostat or on a strong field Mössbauer spectrometer equipped with an Oxford Instruments Spectromag 4000 cryostat containing an 8T split-pair superconducting magnet. Both spectrometers were operated in a constant acceleration mode in transmission geometry. The isomer shifts were referenced against that of a room temperature metallic iron foil. Analysis of the data was performed with the program WMOSS (WEB Research). X-band EPR spectra were recorded on a Bruker ESP-300E EPR spectrometer operating with an ER-4116 dual mode cavity and an Oxford Instruments ESR-9 flow cryostat. Resonances were quantified under nonsaturating conditions by double integration against a 1 mM Cu-EDTA standard.

Purification and Crystal Structure Determination of Apo-T. maritima RimO—Selenomethionine-labeled RimO was purified according to a published procedure (18). Crystals were grown at room temperature using 2 + 2 μl of microbatch reactions under paraffin oil. Subtilisin (Sigma) was added at a concentration of 20 μg/ml to the protein stock solution containing 9.5 mg/ml RimO in 100 mM sodium chloride, 5 mM dithiothreitol, and 10 mM Tris-HCl, pH 7.5, prior to mixing with an equal volume of 40% polyethylene glycol 4000, 100 mM sodium thiosulfate, and 100 mM CAPS, pH 10. Rod-like crystals appeared after 3–4 weeks. Crystals were frozen directly in liquid propane (without cryoprotection) prior to collection of single wavelength anomalous x-ray diffraction data at the selenium absorption edge on Beamline X4A at the National Synchrotron Light Source at the Brookhaven National Laboratory. Diffraction data were integrated and merged using the HKL package (19) followed by the location of most of the selenium sites using BnP (20). SOLVE/RESOLVE (21) was used for phasing and automated model building, which correctly assigned the sequence for 70% of residues in the asymmetric unit. The structure was completed via iterative cycles of model building using XtalView (22) and refinement using CNS (crystallography and NMR system) software (23). 8-Fold noncrystallographic symmetry restraints (300 kcal/Å and $\sigma_B = 2$) were applied for the radical AdoMet domain of the model except during the final cycle of refinement.

Molecular Graphics—Except for Fig. 2*C*, which was prepared using GRASP2 (24), all images were prepared using PyMOL.

RESULTS

Biochemical and Spectroscopic Characterization of T. maritima RimO—A standard purification protocol (15) allowed for the production of a pure protein that migrates as a single band on a denaturating polyacrylamide gel (data not shown), which was confirmed by N-terminal sequencing as being the RimO protein. The apparent molecular mass of RimO determined by analytical gel filtration chromatography (Superdex 200) showed that the protein is mainly a monomer in solution (data not shown). The molecular mass was determined by matrix-assisted laser desorption ionization time-of-flight mass spectrometry to be 49,126 ± 50 Da, in agreement with the mass calculated from the amino acid sequence lacking the N-terminal methionine (49,091 Da). The as-purified protein was light brown in color and found to contain substoichiometric amounts of iron and sulfur atoms (<0.8 iron and sulfur atom/monomer). Holo-RimO could bind up to 7.0 ± 0.5 iron and 8.0 ± 0.7 sulfur atoms/polypeptide chain after anaerobic treatment of the apo-form with an excess of ferrous iron and enzymatically produced sulfide followed by desalting (data not shown).

The UV-visible spectrum of holo-RimO (Fig. 1*A*) displays a broad absorption band centered around 420 nm, which is assigned to sulfur-to-iron charge transfer transitions characteristic of a $[4Fe\text{-}4S]^{2+}$ cluster. This band has an A_{420}/A_{280} ratio of 0.33 ± 0.02 and a molar extinction coefficient at 420 nm of 35 $mM^{-1}\cdot cm^{-1}$ (biological $[4Fe\text{-}4S]^{2+}$ centers typically have $\epsilon_{420} = 15\text{–}17\ mM^{-1}\ cm^{-1}$ on a per cluster basis). In combination with the determination of a ratio of 7–8 iron atoms/holo-RimO, this indicates that the reconstituted enzyme contains two [4Fe-4S] clusters/polypeptide. Upon the addition of dithionite, the absorption decreased over the entire 350–700-nm range (Fig. 1*A*), as expected upon reduction of the chromophore to the $[4Fe\text{-}4S]^{1+}$ state.

The presence of two [4Fe-4S] clusters in the holo-RimO protein was further substantiated by Mössbauer and EPR spectroscopies. Fig. 1*B* illustrates the Mössbauer spectrum of ^{57}Fe reconstituted holo-RimO recorded at 4 K under a field of 50 mT applied perpendicularly to the γ-beam. It is dominated by an asymmetric doublet ($\delta \sim 0.5\ mm\cdot s^{-1}$, $\Delta E_Q \sim 1\ mm\cdot s^{-1}$) flanked by an absorption at $\sim$1.6 $mm\cdot s^{-1}$. Weak additional absorptions appearing as a split peak at $\sim$3 $mm\cdot s^{-1}$ and a shoulder at approximately $-0.8\ mm\cdot s^{-1}$ are attributed to adventitiously bound Fe^{II} ions. The parameters of the main doublet are characteristic of $[4Fe\text{-}4S]^{2+}$ clusters. In agreement with this assignment, experiments performed under a strong magnetic field reveal a diamagnetic behavior. This is also the case for the absorption at 1.6 $mm\cdot s^{-1}$, which must be part of a diamagnetic cluster, although the Mössbauer parameters (δ and ΔE_Q) of the associated quadrupole doublet are unusually large for a $[4Fe\text{-}4S]^{2+}$ cluster. As shown in Fig. 1*B*, the data can be analyzed by taking into account two different $[4Fe\text{-}4S]^{2+}$ clusters. One of them, accounting for 56% of the total iron, was simulated with a quadrupole doublet with parameters ($\delta = 0.45(3)\ mm\cdot s^{-1}$, $\Delta E_Q = 1.04(5)\ mm\cdot s^{-1}$) that are within the range of those

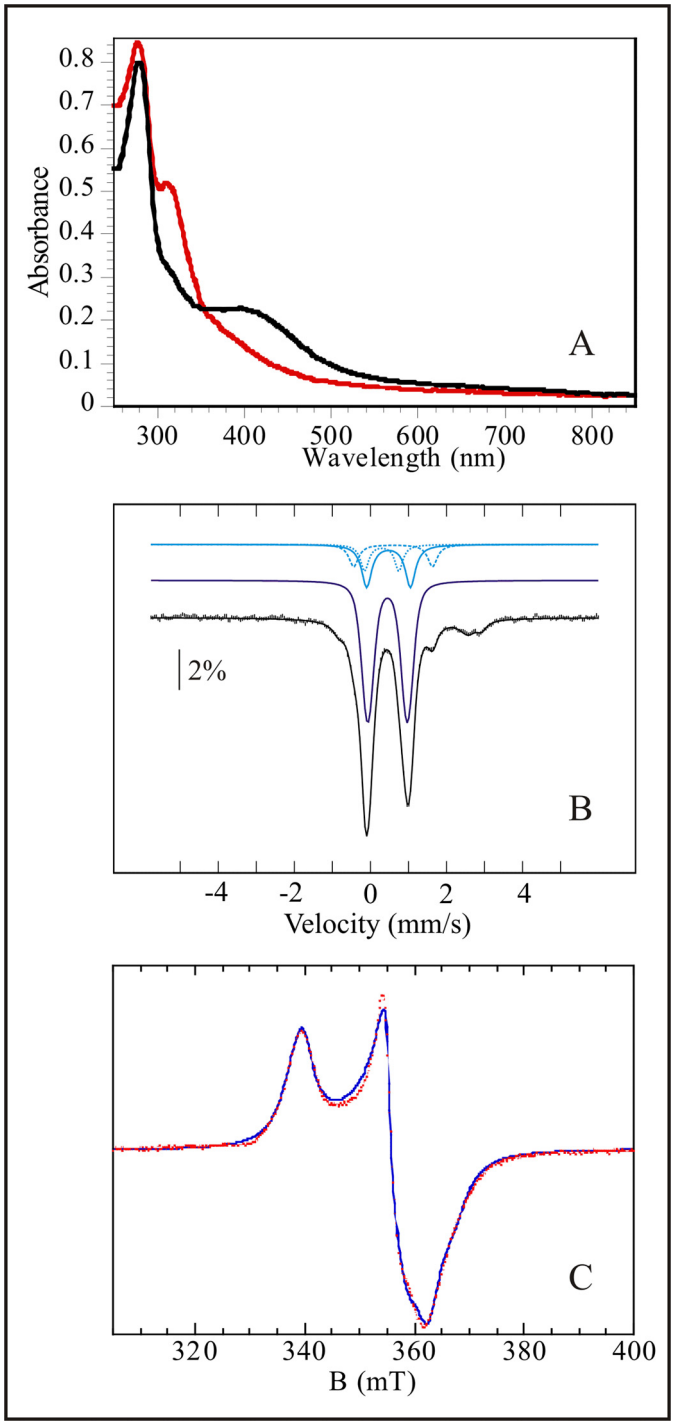

FIGURE 1. **Spectroscopic characterization of holo-RimO.** *A*, UV-visible absorption spectra of oxidized (*black*) and reduced (*red*) forms of holo-RimO (8 μM) in 50 mM NaCl, 50 mM Tris-HCl, pH 8. The absorbance at 314 nm is due to excess dithionite. *B*, Mössbauer spectrum of holo-RimO (288 μM) in the same buffer. The experimental spectrum (*hatched marks*) was recorded at 4.2 K in a magnetic field of 500 mT applied perpendicular to the direction of the γ-beam. The theoretical spectra of the different species are shown as *colored lines* above the experimental spectrum. The *dark blue line* represents a typical $[4Fe\text{-}4S]^{2+}$ cluster, and the *light blue lines* represent the three distinct sites of an atypical $[4Fe\text{-}4S]^{2+}$ cluster composed of a delocalized $Fe^{II}Fe^{III}$ pair (*solid line*) and two distinct Fe centers, one being more ferrous in character (*hatched line*) than the other (*dotted line*). The parameters of all these doublets and their relative absorption intensities are given under "Results." Additionally, two quadrupole doublets (not shown) representing adventitiously bound Fe^{II} were used to simulate the spectrum. The composite spectrum is plotted as a *solid black line* overlaid with the experimental data. *C*, X-band EPR spectrum of reduced holo-RimO (144 μM) in the same buffer. The *dotted red line* shows the g = 2 region of the X-band EPR spectrum recorded on a dithionite reduced sample (natural ^{57}Fe abundance) at 20 K under nonsaturating conditions (0.63-milliwatt microwave power at 9.65 GHz frequency). The *blue line* shows a theoretical simulation with two S = 1/2 species in a 51:49 ratio using a Lorentzian profile. The parameters of species 1 are $g_{1x} = 1.902$, $g_{1y} = 1.930$, $g_{1z} = 2.030$, $w_{1x} = 2.7$ mT, $w_{1y} = 3.4$ mT, and $w_{1z} = 2.2$ mT, whereas those of species 2 are $g_{2x} = 1.879$, $g_{2y} = 1.940$, $g_{2z} = 2.042$, $w_{2x} = 3.4$ mT, $w_{2y} = 1.1$ mT, and $w_{2z} = 3.1$ mT (half-width at half-maximum).

observed for typical $[4Fe\text{-}4S]^{2+}$ clusters. The other one, accounting for 32% of total iron, was simulated with three different quadrupole doublets with relative signal intensity ratios 2:1:1. The first doublet with double intensity has parameters ($\delta = 0.48$ (6) mm·s^{-1}, $\Delta E_Q = 1.15$ (9) mm·s^{-1}) consistent with a valence-delocalized $Fe^{II}Fe^{III}$ pair within the cluster. By contrast, the two remaining iron sites in the cluster are distinct, one of them having a more ferrous character ($\delta = 0.60$ (4) mm·s^{-1}, $\Delta E_Q = 2.07$ (8) mm·s^{-1}) than the other ($\delta = 0.3$ (1) mm·s^{-1}, $\Delta E_Q = 0.9$ (2) mm·s^{-1}). This increased ferrous character yields a quadrupole doublet with larger δ and ΔE_Q parameters, which makes it noticeably distinct in the Mössbauer spectrum. Similar parameters have been reported recently for $[4Fe\text{-}4S]^{2+}$ clusters containing a unique Fe site (25–27). The Mössbauer spectra of ^{57}Fe reconstituted dithionite-reduced holo-RimO are split magnetically and could be fitted with a set of parameters typical for $[4Fe\text{-}4S]^{1+}$ clusters with S = ½ ground state (supplemental Fig. 4).

The EPR spectrum of the corresponding unenriched RimO comprises two components. A weak signal at low field, around g ~ 4, corresponding to an S > ½ integer spin system (supplemental Fig. 5) and a major slightly rhombic component at g ~ 2 that is clearly associated with an S = ½ spin state (Fig. 1*C*). Interestingly, all attempts to simulate the g ~ 2 signal with a single spin ½ failed to reproduce the perpendicular region (supplemental Fig. 6). By contrast, taking into account two slightly different S = ½ spins in a 1:1 ratio allowed us to reproduce the experimental spectrum. As shown in supplemental Fig. 7, the EPR spectrum of ^{57}Fe-enriched, dithionite-reduced holo-RimO could be simulated with the same set of parameters except for increased line widths and a species ratio of 59:41 (1.44). This ratio is consistent with that derived from the Mössbauer analysis of a sample from the same preparation before dithionite reduction 56:32 (1.75). The difference between the ^{57}Fe-enriched and the unenriched samples probably originates from the different reconstitution procedures (see "Material and Methods"). Thus the EPR analysis also supports the presence of two $[4Fe\text{-}4S]^{1+}$ in reduced holo-RimO.

Crystal Structure of the Radical AdoMet and TRAM Domains of Apo-T. maritima RimO—We succeeded in growing diffraction-quality crystals of apo-RimO only in the presence of small amounts of subtilisin (28), suggesting that cleavage of some flexible protein segments was required to enable the formation of a well ordered crystal lattice. Although the central radical AdoMet and C-terminal TRAM domains were visualized in the resulting 2.0 Å crystal structure (Table 1, Scheme 1*B*, and Fig. 2, *A–D*), no electron density was observed for the N-terminal UPF0004 domain, suggesting that it had been removed by the subtilisin treatment. Whether or not cleavage occurred, the

TABLE 1
Summary of crystallographic data for *T. maritima* RimO[a]

Space Group	**P1**
Cell parameters (Å)	**88.6 x 88.7 x 96.0 Å (91.0°, 90.0°, 89.9°)**
Resolution (Å)	**29.9 - 2.00 (2.07-2.00)**
Number of reflections	**61,067**
Mean redundancy	**1.7**
$\langle I/s_I \rangle$	**14.2 (3.5)**
R_{sym} (%) [b]	**6.6 (36.0)**
Completeness (%)	**96.6 (96.0)**
R_{work} (%) [c]	**21.2 (23.4)**
R_{free} (%) [c]	**25.1 (27.3)**
Rmsd in bond lengths (Å)	**0.006**
Rmsd in bond angles (°)	**1.1**
Model contents:	
Protein residues	**A: 135-148, 162-329, 341-430 B,E,H: 136-147, 162-329, 341-430 C,D,F,G: 136-146, 162-329, 341-430**
Heteroatoms	**4 (3-cyclohexyl-1-propylsufonic acid) 1442 H_2O**
Ramachandran distribution:	
Core	**91.3%**
Additionally allowed	**9.0%**
Generously allowed	**0%**
Disallowed	**0.8%**

[a] **The numbers in parenthesis are for the highest resolution shell.**

[b] $R_{merge} = \sum_h \sum_i |I_{hi} - \langle I_h \rangle| \Big/ \sum_h \sum_i I_{hi}$

[c] $R = \sum_h |F_h^o - F_h^c| \Big/ \sum_h F_h^o$

failure to observe it in the crystal structure indicates that it is loosely associated with the other domains in apo-RimO. In addition, no electron density was observed for residues 149–161 and 330–340 in the radical AdoMet domain, meaning that these loops also may have been cleaved by subtilisin. The first of these missing segments contains the bulk of the [4Fe-4S]-ligating Cys-*XXX*-Cys-*XX*-Cys triad (at residues 148–155), indicating that this loop is likely to be disordered in the absence of the [4Fe-4S] cluster. The radical AdoMet domain in RimO (*yellow*, *cyan*, and *blue* in Scheme 1*B* and Fig. 2*A*) contains six parallel β-strands and seven α-helices, which form an open or incomplete triose-phosphate isomerase barrel equivalent to that found in other radical AdoMet enzymes (29) such as MoaA (involved in molybdenum cofactor biosynthesis (30)) (Fig. 2*E*). According to the program DALI, the most closely related domain of known structure is found in oxygen-independent coproporphyringogen III (PDB ID 1OLT, *Z*-score = 11.7, and 4.2 Å r.m.s.d. for alignment of 211 Cαs with 18% sequence identity) (31). Other radical AdoMet domains show similarly high scores, including MoaA (30) (PDB ID 2FB2, *Z*-score = 9.9, and 4.2 Å r.m.s.d. for alignment of 185 α carbons with 9% sequence identity). MoaA, which is involved in molybdenum cofactor biosynthesis (30), provides the most informative comparison with RimO because it also contains two [4Fe-4S] clusters, and its anaerobic crystal structure has been determined with both clusters bound, as well as its primary substrate (GTP) and AdoMet co-substrate. The corresponding structural superposition (Fig. 2, *E* and *F*) provides insight into the organization of the active site in RimO, including most importantly the likely positioning of its AdoMet co-substrate, the S12 substrate, and two [4Fe-4S] clusters.

Although the curvature of the incomplete triose-phosphate isomerase barrel varies somewhat in these homologous domains, they share all of the secondary structural elements except the final long α-helix at the C terminus of the radical AdoMet domain in RimO. However, most contain additional C-terminal secondary structural elements that cover the concave surface of the incomplete triose-phosphate isomerase barrel to form a closed binding site for the small molecule substrates of these enzymes (*e.g.* as shown for the GTP substrate in MoaA in Fig. 2, *E* and *F*). Positioning a macromolecular substrate like the S12 protein in an equivalent location requires some modification of the molecular architecture. Consistent with this inference, the protein segments binding GTP in MoaA are missing from the radical AdoMet domain of RimO, resulting in solvent exposure of the concave surface of its open triose-phosphate isomerase barrel. Based on the fact that, in MoaA, the GTP substrate binds to this surface (Fig. 2*E*), the S12 protein substrate for RimO and the tRNA substrate for the paralogous MiaB enzyme (13) are both likely to bind at the same site.

This inference is strongly supported by the location of the TRAM domain in RimO (Fig. 2, *A* and *C*) as well as its electrostatic characteristics (Fig. 2*B*). TRAM domains are well known to bind RNA molecules (12, 14); thus the TRAM domain in MiaB has long been assumed to participate in binding of its tRNA substrate (12). Given the uniformly strong sequence homology throughout the RimO and MiaB sequences, the TRAM domain in both of these paralogous enzymes is expected to interact in the same geometry with the radical AdoMet domain. In RimO, the TRAM domain (Fig. 2, *A* and *D–F*, *red*) is bound at the distal edge of the concave surface of the radical AdoMet domain, strongly supporting our hypothesis that macromolecular substrates bind to this surface in RimO/MiaB family enzymes.

The five-stranded anti-parallel β-barrel topology of the TRAM domain of RimO is equivalent to that of other TRAM domains of known structure (Fig. 2*D*). According to DALI, the most closely related domain is found in a AdoMet-dependent methyltransferase of unknown function (PDB ID 1K3R, *Z*-score = 8.2, and 1.7 Å r.m.s.d. for alignment of 53 Cαs with 8% sequence identity) (32). Other TRAM domains show similarly high scores, including that in the 23 S ribosomal RNA methyltransferase RumA (PDB ID 1UWV, *Z*-score = 7.4, and 1.8 Å r.m.s.d. for alignment of 52 Cαs with 17% sequence identity) (33).

Although most TRAM domains are believed to bind negatively charged RNA molecules, as hypothesized to occur in MiaB (12), the binding specificity of this domain should presumably be altered in RimO to mediate interaction with the positively charged S12 protein. Consistent with this assumption, the putative substrate-binding surface of the TRAM domain in RimO is strongly acidic (negatively charged) (Fig. 2*C*). This electrostatic environment is attributable in large part to the presence of acidic residues in the TRAM domain that are conserved in RimO orthologs but not in paralogous tRNA-

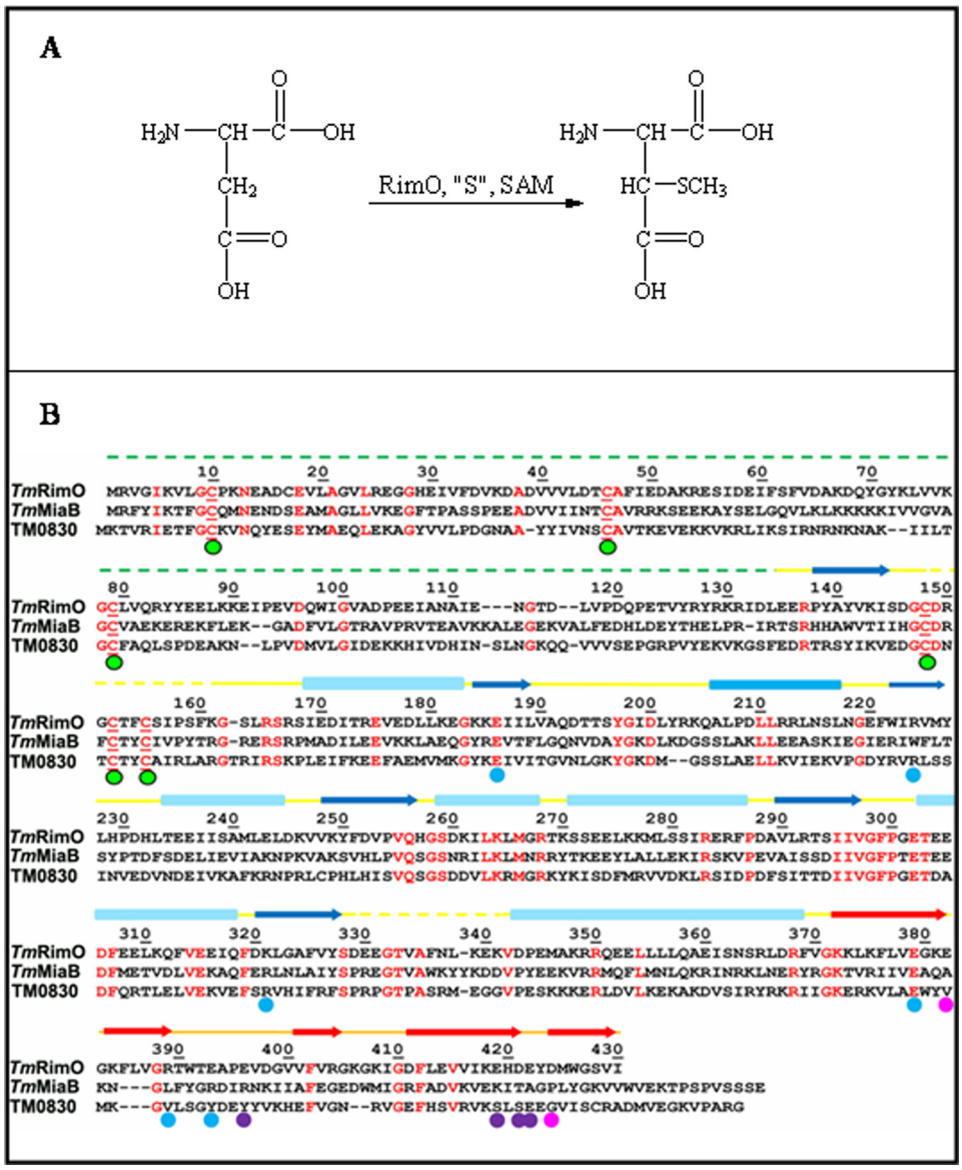

SCHEME 1. *A*, the reaction catalyzed by RimO; "*S*" represents the sulfur atom donor. *B*, sequence alignment of *T. maritima* RimO (TM1862), MiaB (TM0653), and TM0830 performed using T-COFFEE (41). TM0830 is a third paralog with equivalent domain organization also encoded in the genome of *T. maritima*. Identical residues in all three paralogs are shown in *red*. A structural schematic is shown above the alignment with α-helices and β-strands represented by *rectangles* and *arrows*, respectively, and backbone segments not observed in the crystal structure of apo-*T. maritima* RimO are indicated by *dotted lines*. The UPF0004 domain is shown in *green*, the radical AdoMet domain in *yellow* and *blue*, and the TRAM domain in *orange* and *red*. (None of the UPF0004 domain was observed in the crystal structure.) The *green circles* below the alignment indicate the invariant cysteines, and the *cyan circles* indicate conserved residues making salt bridges in the interface between the radical AdoMet and TRAM domains. The *magenta* and *purple circles* indicate, respectively, invariant and conserved acidic residues among RimO orthologs (data not shown) on the surface of the TRAM domain proximal to the active site of the radical AdoMet domain.

binding enzymes like MiaB (14) (as indicated in Scheme 1*B*). Construction of a homology model of MiaB based on the coordinates of RimO indicates that the corresponding region of MiaB is basic or positively charged instead of acidic (data not shown), consistent with binding of its tRNA substrate on the homologous surface. Therefore, our partial structure of RimO, combined with analyses of homologous proteins, provides insight into the likely binding geometry of its macromolecular substrate relative to the location of its radical AdoMet active site (Fig. 2, *E* and *F*).

This crystal structure furthermore provides insight into the locations of the two [4Fe-4S] clusters that we have shown to be present in RimO. Although only the first Cys residue (Cys-148) in the conserved cysteine triad in the radical AdoMet domain is observed in our RimO structure, it is located very close to the homologous residue in MoaA (Cys-24) (Fig. 2, *E* and *F*). Therefore, the [4Fe-4S] clusters bound to the radical AdoMet domains in both enzymes are likely to be located at equivalent sites. However, the second [4Fe-4S] cluster in MoaA is located in the region where the S12 substrate protein is hypothesized to bind to RimO (Fig. 2, *E* and *F*). Therefore, the second [4Fe-4S] cluster in RimO, which is bound to the N-terminal UPF004 domain, is likely to occupy a different location relative to the conserved AdoMet and [4Fe-4S] binding sites in its radical AdoMet domain. Substantial stereochemical differences are thus likely in the Michaelis complexes of RimO *versus* MoaA, despite the homology of their radical AdoMet domains.

In Vitro Methylthiolation Activity of T. maritima RimO Enzyme—Previous work done by Anton *et al.* (5) shows that complementation of the *E. coli rimO* knock-out strain with the wild-type *rimO* gene (*yliG*) restores the production of ms-D89 *in vivo*. To investigate the enzymatic conversion of Asp-89 to ms-D89 *in vitro*, we used a 20-mer peptide substrate with the sequence LVRGGRVK**D**LPGVRYKIIRG, corresponding to the sequence surrounding Asp-89 (in bold) of the S12 protein. The enzymatic reaction was carried out and treated as described under "Materials and Methods." Fig. 3 shows the UV chromatograms of the peptide before (Fig. 3*A*) and after (Fig. 3*B*) reaction with holo-RimO. In Fig. 3*B*, in addition to the peak of the unmodified peptide eluting at ~17 min, two new peaks are apparent after a 60-min reaction with holo-RimO; one of these is only partially resolved and elutes at ~18 min, corresponding to compound **1**, whereas the other is well separated from that of the unmodified peptide and elutes at ~24 min, corresponding to compound **2**. Fig. 3*C* shows the mass spectrum of the solution in the +5, +4, and +3 charge states. The calculated molecular weight of the corre-

sponding peaks was found by MS1 to be 2253.1 for the unmodified peptide (Fig. 3*C*, *red*; theoretical, 2252.8), 2300 for compound **1** (Fig. 3*C*, *black*), and 2346.5 for compound **2** (Fig. 3*C*, *blue*). The latter two values are consistent with the addition to the unmodified peptide of one (+46) and two (+2 × 46) methylthio groups, respectively. Mass spectrometric sequencing (MS2) unambiguously established that the methylthio group of compound **1** is located exclusively at the aspartate residue of the peptide (supplemental Fig. 8, *A* and *B*). This methylthiolation is likely to occur on the 3-carbon position of the aspartate residue as suggested previously (4). The MS2 of compound **2** failed to localize the second methylthiolation. However the presence of (y11)+ ion indicates that the reaction occurred between y1 and y10 (supplemental Fig. 8*C*). More work is needed to localize precisely the site(s) of this modification. No reaction was observed in the absence of holo-RimO, AdoMet, or dithionite. Because of similar charge state distributions of the peptide and its derivatives, an estimation of the yield of the methylthiolation reaction by holo-RimO was possible on the basis of the area of the HPLC-MS peaks (see "Materials and Methods"). Under the incubation conditions used, 0.3 nmol of holo-RimO could insert 0.8 nmol of the sulfur atom into the substrate, yielding ~0.6 nmol of products **1** + **2**. It is important to note that as no external sulfur source was added in the assay mixture, the enzyme is not expected to turn over under these conditions. This result suggests that during reconstitution of the Fe-S clusters, holo-RimO has incorporated more than two sulfur atoms available for the methylthiolation reaction.

Analysis of the reaction mixture at 260 nm on a C18 column revealed the presence of five compounds. The identity of each peak was clearly established by their HPLC retention times with respect to those of authentic commercial compounds (supplemental Fig. 9). Besides the remaining AdoMet, four new peaks are apparent, two originating from heat-degraded AdoMet (adenine and methythioadenosine), the two other being the by-products of the RimO reaction (AdoH and *S*-adenosylhomocysteine). The time course of the produc-

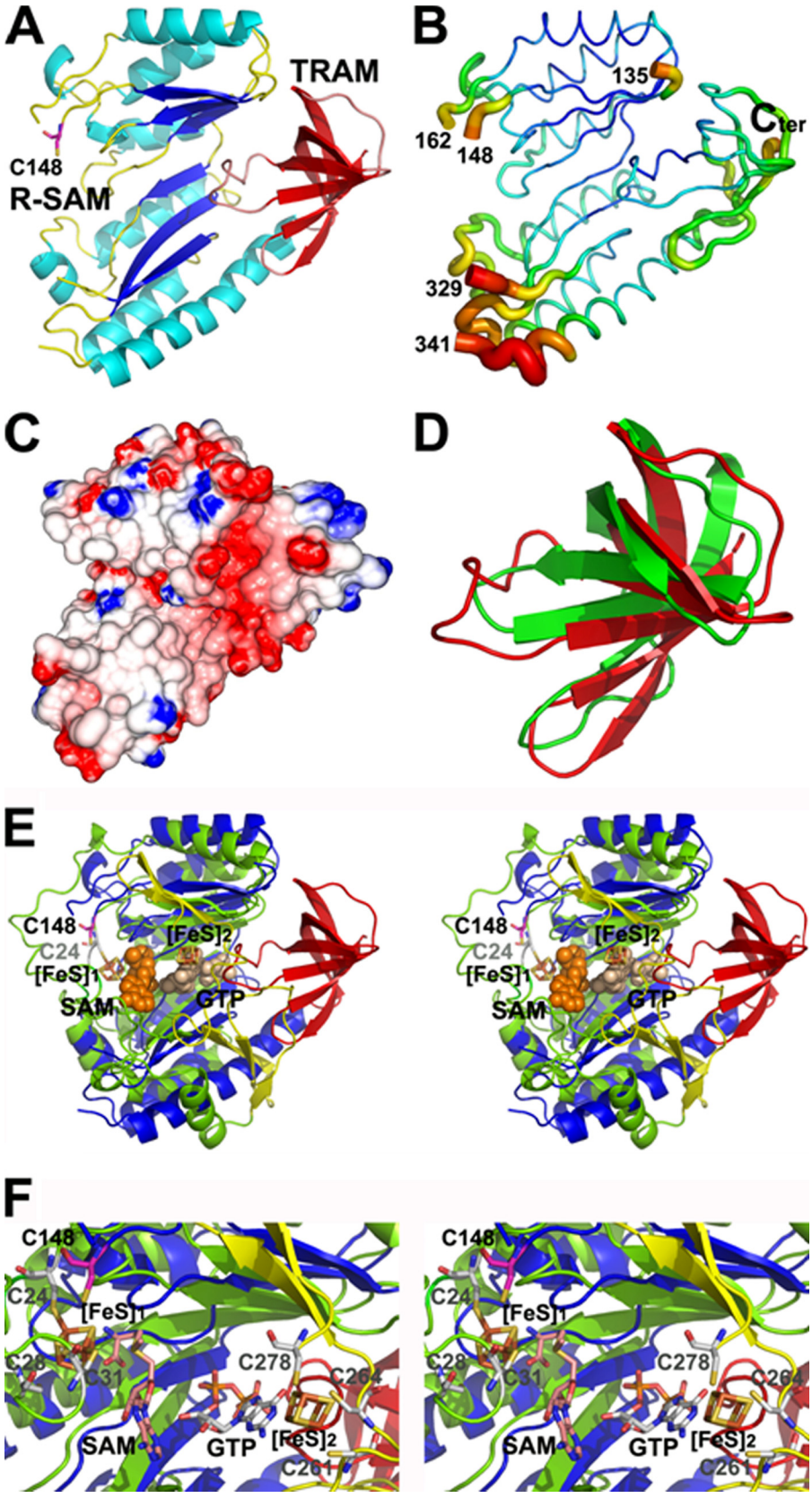

tion of these five compounds is given in supplemental Fig. 10. The amounts of the by-products of the RimO reaction (AdoH and *S*-adenosylhomocysteine) formed during a 70-min time course are reported in Table 2. It is noteworthy that whereas *S*-adenosylhomocysteine is produced in an ~1.5-fold excess (1.19/0.8) with regard to the thiolated products, the AdoH/thiolated products ratio culminates in a value of about 5 (4.04/0.8). Moreover, whereas AdoH production is strictly dependent on the presence of the peptide substrate, *S*-adenosylhomocysteine is partially formed even in the absence of the latter (data not shown).

DISCUSSION

In this study, we have shown that holo-RimO from *T. maritima* can accommodate two [4Fe-4S]$^{2+/1+}$ centers and confirmed, via an *in vitro* assay, that this radical AdoMet enzyme catalyzes the methylthiolation of a peptide-bound aspartate residue (5). During the submission process of the present work, a closely related paper appeared in the literature, which presents a spectroscopic and functional characterization of the RimO enzyme from *E. coli* in general agreement with our data (34). However, in this study the spectroscopic characterization suffers from an apparent lack of homogeneity in the reconstituted samples, which contain significant amount of adventitious iron. The high iron content may explain the broad absorption in the Mössbauer spectrum. In contrast, the more homogenous preparations of *T. maritima* RimO allow for clear spectroscopic differentiation between the two [4Fe-4S] clusters. However, further studies are needed to assign each spectroscopic signature to its cognate cluster. Furthermore, the *T. maritima* RimO is much more active than the *E. coli* RimO. Finally, our study provides the first partial structural characterization of the enzyme.

The absolute requirement for two iron-sulfur clusters in enzymes involved in C–H to C–S bond conversion reactions is thus a feature that does not suffer any exception so far. Indeed, the same cluster content has been found in the radical AdoMet enzymes biotin synthase (BioB) (35) and lipoate synthase (LipA) (36), a tRNA methylthioltransferase (MiaB) (13), and now RimO. However variations have been observed regarding the type of clusters bound to the proteins. Although they all contain a [4Fe-4S] cluster bound to cysteines of a Cys-*XXX*-Cys-*XX*-Cys motif and capable of reducing AdoMet, the second cluster can be a [2Fe-2S] cluster (BioB) or a [4Fe-4S] center (LipA, MiaB, and RimO). This observation has led to the general hypothesis that, in all of these enzymes, the second cluster, or activated derivatives of it, serves as the source of sulfur atoms during the thiolation reaction (11).

The RimO-catalyzed reaction is thus supposed to proceed through following steps: (i) AdoMet reductive cleavage promoted by the radical AdoMet cluster to generate a 5′-deoxyadenosyl radical, Ado$^{\bullet}$; (ii) selective H atom abstraction at the 3-carbon of the aspartate substrate by Ado$^{\bullet}$; (iii) reaction of the resulting intermediate radical with second [4Fe-4S] cluster, through a thus far ill defined mechanism, to generate the C–S bond; (iv) methylation at the introduced sulfur atom, most probably through the reaction with the electrophilic methyl group of a second AdoMet molecule. Further experiments are needed to substantiate this mechanism. Most of the radical AdoMet enzymes that have been functionally studied display a decoupled AdoMet cleavage, which refers to a reductive cleavage of AdoMet in the absence of substrate, or a reductive cleavage of AdoMet that exceeds the stoichiometry required for catalysis (37, 38). In the case of RimO this decoupling is observed only in the presence of the substrate (AdoH/product around 5). The same behavior has also been observed with the *E. coli* enzyme (34). Together with the unexpected formation of a bismethylthiolated product, this may be a consequence of using a minimal substrate (a peptide in place of the S12 protein) that does not allow a strict control of the outcome of the reaction. Finally, it is interesting to note that one molecule of *T. maritima* RimO is able to insert a total of 2 equivalents of the methylthio group into the substrate, whereas the *E. coli* enzyme produces only a 0.12 equivalent (34). However, as with BioB, LipA, and MiaB, there is a need to find the conditions for multiple turnovers. In addition to AtsB, which is involved in the maturation of sulfatases, RimO constitutes the second example of a radical AdoMet enzyme involved in protein modification (39).

RimO displays many similarities to MiaB. First, like MiaB, it is a bifunctional enzyme, catalyzing the same two reactions: a radical insertion of sulfur atoms in the substrate and a methylation at the introduced sulfur atoms. In the case of RimO some molecules of the substrate have been methylthiolated twice, possibly because of altered interactions of the peptide substrate with RimO as compared with that of the complete S12 protein. Second, as in the case of MiaB, the two [4Fe-4S] clusters in RimO display different spectroscopic signatures; further experiments are needed to assign these signatures to specific clusters. The clusters are more differentiated in the case of RimO, as they can be resolved spectroscopically in both Mössbauer and EPR spectra. The third common characteristic of RimO and MiaB is the conservation of a TRAM domain at the C terminus of the protein. This domain organization is intriguing because TRAM motifs are known to specifically recognize nucleic acids (33). It

FIGURE 2. **Crystal structure of the radical AdoMet and TRAM domains in apo-RimO from *T. maritima*.** *A*, schematic diagram with the radical *S*-adenosylmethionine (*R-SAM*) domain colored *cyan*, *blue*, and *yellow* and the TRAM domain colored *red* and *orange*. Invariant residue Cys-148, which probably ligates one [4Fe-4S] cluster in holo-RimO, is shown in *ball-and-stick* representation. *B*, an equivalent view of the structure with the color and thickness of the backbone worm representing backbone B-factors, which measure the degree of positional disorder in the crystal. The color ramp runs from *blue* for the lowest B-factors (10.7 Å^2) to *red* for the highest (69.1 Å^2). The C terminus is labeled *Cter*, and *residue numbers* are given for all other termini of the observed polypeptide segments. *C*, electrostatic surface potential of RimO, with *blue* and *red* representing acidic and basic regions, respectively, and fully saturated colors indicating a potential of ±14 kT at an ionic strength of 100 mM (24). *D*, structural superposition of the TRAM domains in RimO (*red*) and RumA (*green*) as aligned by DALI. *E*, stereopair showing structural superposition of the radical AdoMet domains in RimO (*blue* and *red*) and MoaA (*green* and *yellow*) as aligned by DALI. The AdoMet co-substrate (*orange*) and GTP substrate (*wheat*) in MoaA are shown in *space-filling* representations, and its [4Fe-4S] clusters and Cys-24 (equivalent to Cys-148 in RimO) are shown in *ball-and-stick* representations. The C-terminal α-helices in MoaA, which pack on the surface of the *yellow* β-sheets, have been omitted to improve clarity. *F*, stereopair showing a close-up view of the active site in the same structural superposition.

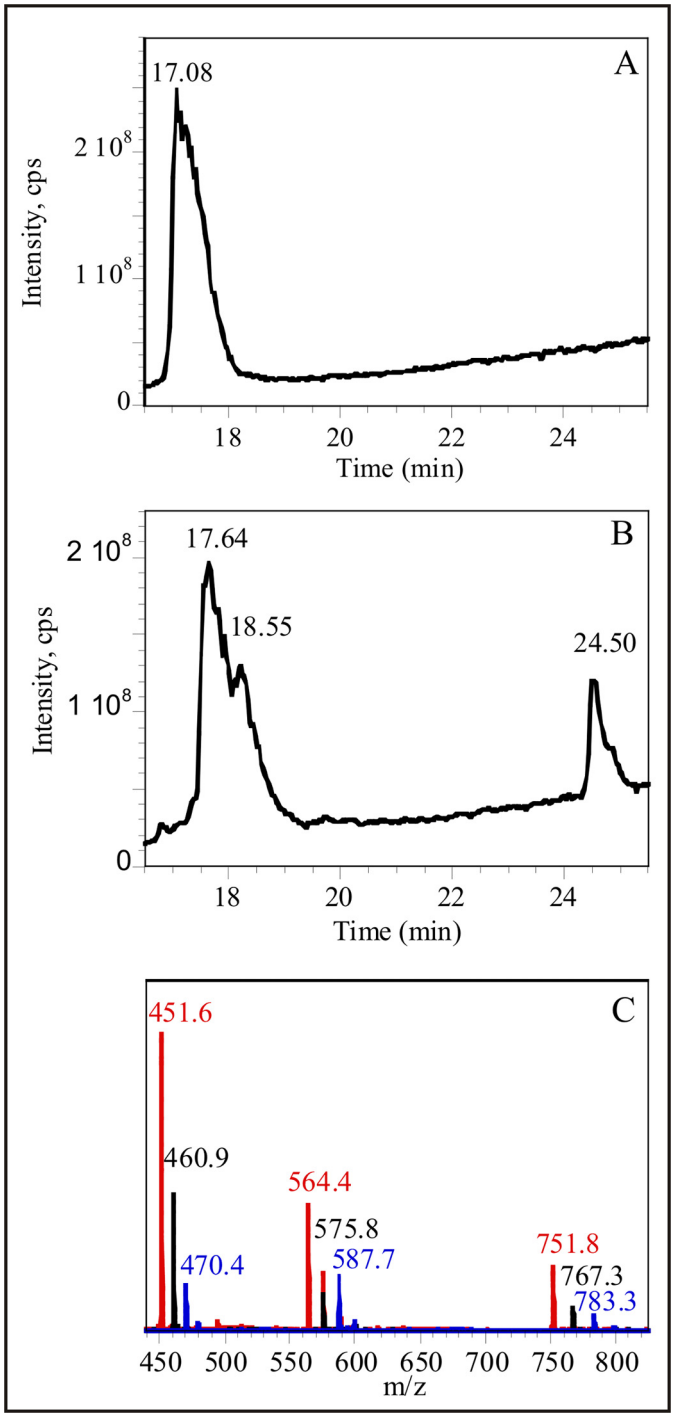

FIGURE 3. **HPLC-MS identification of enzymatic reaction products.** *A*, total ion-current chromatogram for the 20-mer peptide without enzyme treatment. *B*, equivalent chromatogram after reaction of the peptide with holo-RimO. The peaks at 18.55 and 25.50 min correspond to monomethylthio and bismethylthio derivatives, respectively. *C*, mass spectra of the unmodified peptide (*red*), monomethylthio derivative (*black*), and bismethylthio derivative (*blue*) showing +5, +4, and +3 charge states.

was thus hypothesized initially that the interaction between RimO and its protein substrate involves the participation of ribosomal nucleic acids (5). However, our data show that substrate recognition can take place in the absence of any nucleic acid. Reinforcing this result, the partial structure of RimO presented here shows that this domain displays a highly negatively charged surface, suggesting a direct binding of the very basic S12 substrate protein. Interestingly, previous studies have shown that some ribosomal proteins, among these S12 itself, adopt an L-shaped quaternary structure reminiscent of that of tRNAs (40). A homology-based structural model of MiaB (data not shown) indicates a complete inversion of polarity in the equivalent region in this protein, in agreement with MiaB binding a tRNA substrate at the equivalent site.

TABLE 2

Time courses for the formation of the by-products in the reaction of RimO with the peptide substrate

The assay mixture (50 μl) contained 30 μM of 20-mer peptide substrate and 6 μM of reconstituted RimO protein in 0.2 mM SAM, 2 mM dithionite, and 100 mM Tris-Cl, pH 7.5. The reaction was carried out and treated as described under "Materials and Methods." SAH, *S*-adenosylhomocysteine.

Incubation reaction time	AdoMet	SAH	AdoH
min	*nmol*	*nmol*	*nmol*
3	7.87	0.18	0.53
15	6.27	0.49	1.87
25	5.33	0.68	2.59
45	4.06	0.92	3.29
68	3.41	1.19	4.04

Binding of the S12 and tRNA substrates to the TRAM domains in RimO and MiaB will position them proximal to the conserved site of AdoMet binding in the radical AdoMet domain (Fig. 2*E*), as expected, to enable hydrogen atom abstraction from the substrate by the adenonsyl radical intermediate generated from AdoMet. This likely binding site for macromolecular substrates on the concave surface of the radical AdoMet domain coincides with the location of the binding cavities for the small molecule substrates of enzymes like BioB (not shown) and MoaA (Fig. 2*E*). The binding of macromolecular substrates at this site in RimO/MiaB family enzymes explains the absence of the additional secondary structural elements found on this surface in BioB, MoaA, and other radical AdoMet enzymes that process small molecule substrates. It is noteworthy that these elements bind the second [Fe-S] clusters in both BioB (not shown) and MoaA (Fig. 2*E*). Their absence in RimO and MiaB, combined with the occupancy of this region by the macromolecular substrates, will prevent the second [Fe-S] from binding to a comparable site in these enzymes. Therefore, the [4Fe-4S] cluster bound to the UPF0004 domain in RimO and MiaB is likely to interact with the radical AdoMet domain active site in a substantially different geometry compared with the second clusters in BioB and MoaA. Our coordinated structural and mechanistic characterization of RimO and MiaB should continue to provide new insight into sulfur atom insertion into macromolecular substrates.

Acknowledgments—We thank Sylvie Kieffer-Jaquinod (CEA-iRTSV-EDyP-Grenoble) for MS2 analysis, Bernard Dublet for matrix-assisted laser desorption ionization time-of-flight experiments, and Fabien Pierrel for cloning the rimO gene from T. maritima. The crystallographic work was supported by National Institutes of Health Protein Structure Initiative Grants GM074958 and GM062413 to the Northeast Structural Genomics Consortium.

REFERENCES

1. Carroll, A. J., Heazlewood, J. L., Ito, J., and Millar, A. H. (2008) *Mol. Cell. Proteomics* **7**, 347–369

2. Polevoda, B., and Sherman, F. (2007) *Mol. Microbiol.* **65,** 590–606
3. Dong, H., and Kurland, C. G. (1995) *J. Mol. Biol.* **248,** 551–561
4. Kowalak, J. A., and Walsh, K. A. (1996) *Protein Sci.* **5,** 1625–1632
5. Anton, B. P., Saleh, L., Benner, J. S., Raleigh, E. A., Kasif, S., and Roberts, R. J. (2008) *Proc. Natl. Acad. Sci. U. S. A.* **105,** 1826–1831
6. Sofia, H. J., Chen, G., Hetzler, B. G., Reyes-Spindola, J. F., and Miller, N. E. (2001) *Nucleic Acids Res.* **29,** 1097–1106
7. Fontecave, M., Mulliez, E., and Ollagnier-de-Choudens, S. (2001) *Curr. Opin. Chem. Biol.* **5,** 506–511
8. Frey, P. A., Hegeman, A. D., and Ruzicka, F. J. (2008) *Crit. Rev. Biochem. Mol. Biol.* **43,** 63–88
9. Fontecave, M., Mulliez, E., and Atta, M. (2008) *Chem. Biol.* **15,** 209–210
10. Fontecave, M., Ollagnier-de-Choudens, S., and Mulliez, E. (2003) *Chem. Rev.* **103,** 2149–2166
11. Booker, S. J., Cicchillo, R. M., and Grove, T. L. (2007) *Curr. Opin. Chem. Biol.* **11,** 543–552
12. Anantharaman, V., Koonin, E. V., and Aravind, L. (2001) *FEMS Microbiol. Lett.* **197,** 215–221
13. Hernández, H. L., Pierrel, F., Elleingand, E., García-Serres, R., Huynh, B. H., Johnson, M. K., Fontecave, M., and Atta, M. (2007) *Biochemistry* **46,** 5140–5147
14. Lee, T. T., Agarwalla, S., and Stroud, R. M. (2005) *Cell* **120,** 599–611
15. Pierrel, F., Hernandez, H. L., Johnson, M. K., Fontecave, M., and Atta, M. (2003) *J. Biol. Chem.* **278,** 29515–29524
16. Fish, W. W. (1988) *Methods Enzymol.* **158,** 357–364
17. Beinert, H. (1983) *Anal. Biochem.* **131,** 373–378
18. Forouhar, F., Hussain, M., Farid, R., Benach, J., Abashidze, M., Edstrom, W. C., Vorobiev, S. M., Xiao, R., Acton, T. B., Fu, Z., Kim, J. J., Miziorko, H. M., Montelione, G. T., and Hunt, J. F. (2006) *J. Biol. Chem.* **281,** 7533–7545
19. Otwinowski, Z., and Minor, W. (1997) *Methods Enzymol.* **276,** 307–326
20. Miller, R., Shah, N., Green, M. L., Furey, W., and Weeks, C. M. (2007) *J. Appl. Crystallogr.* **40,** 938–944
21. Terwilliger, T. C. (2003) *Methods Enzymol.* **374,** 22–37
22. McRee, D. E. (1999) *J. Struct. Biol.* **125,** 156–165
23. Brunger, A. T., Adams, P. D., Clore, G. M., DeLano, W. L., Gros, P., Grosse-Kunstleve, R. W., Jiang, J. S., Kuszewski, J., Nilges, M., Pannu, N. S., Read, R. J., Rice, L. M., Simonson, T., and Warren, G. L. (1998) *Acta Crystallogr.* **54,** 905–921
24. Petrey, D., and Honig, B. (2003) *Methods Enzymol.* **374,** 492–509
25. Walters, E. M., Garcia-Serres, R., Jameson, G. N., Glauser, D. A., Bourquin, F., Manieri, W., Schürmann, P., Johnson, M. K., and Huynh, B. H. (2005) *J. Am. Chem. Soc.* **127,** 9612–9624
26. Seemann, M., Janthawornpong, K., Schweizer, J., Böttger, L. H., Janoschka, A., Ahrens-Botzong, A., Tambou, E. N., Rotthaus, O., Trautwein, A. X., and Rohmer, M. (2009) *J. Am. Chem. Soc.* **131,** 13184–13185
27. Yang, J., Naik, S. G., Ortillo, D. O., García-Serres, R., Li, M., Broderick, W. E., Huynh, B. H., and Broderick, J. B. (2009) *Biochemistry* **48,** 9234–9241
28. Bai, Y., Auperin, T. C., and Tong, L. (2007) *Acta Crystallogr. Sect. F Struct. Biol. Cryst. Commun.* **63,** 135–138
29. Nicolet, Y., and Drennan, C. L. (2004) *Nucleic Acids Res.* **32,** 4015–4025
30. Hänzelmann, P., and Schindelin, H. (2006) *Proc. Natl. Acad. Sci. U. S. A.* **103,** 6829–6834
31. Layer, G., Moser, J., Heinz, D. W., Jahn, D., and Schubert, W. D. (2003) *EMBO J.* **22,** 6214–6224
32. Zarembinski, T. I., Kim, Y., Peterson, K., Christendat, D., Dharamsi, A., Arrowsmith, C. H., Edwards, A. M., and Joachimiak, A. (2003) *Proteins* **50,** 177–183
33. Lee, T. T., Agarwalla, S., and Stroud, R. M. (2004) *Structure* **12,** 397–407
34. Lee, K. H., Saleh, L., Anton, B. P., Madinger, C. L., Benner, J. S., Iwig, D. F., Roberts, R. J., Krebs, C., and Booker, S. J. (2009) *Biochemistry* **48,** 10162–10174
35. Berkovitch, F., Nicolet, Y., Wan, J. T., Jarrett, J. T., and Drennan, C. L. (2004) *Science* **303,** 76–79
36. Cicchillo, R. M., Iwig, D. F., Jones, A. D., Nesbitt, N. M., Baleanu-Gogonea, C., Souder, M. G., Tu, L., and Booker, S. J. (2004) *Biochemistry* **43,** 6378–6386
37. Chandor-Proust, A., Berteau, O., Douki, T., Gasparutto, D., Ollagnier-de-Choudens, S., Fontecave, M., and Atta, M. (2008) *J. Biol. Chem.* **283,** 36361–36368
38. Duschene, K. S., Veneziano, S. E., Silver, S. C., and Broderick, J. B. (2009) *Curr. Opin. Chem. Biol.* **13,** 74–83
39. Benjdia, A., Leprince, J., Sandström, C., Vaudry, H., and Berteau, O. (2009) *J. Am. Chem. Soc.* **131,** 8348–8349
40. Selmer, M., Al-Karadaghi, S., Hirokawa, G., Kaji, A., and Liljas, A. (1999) *Science* **286,** 2349–2352
41. Notredame, C., Higgins, D. G., and Heringa, J. (2000) *J. Mol. Biol.* **302,** 205–217